Heavy-ion excitation and photon decay of giant resonances in ^{208}Pb

J. R. Beene, F. E. Bertrand, M. L. Halbert, R. L. Auble, D. C. Hensley, D. J. Horen, R. L. Robinson, R. O. Sayer, and T. P. Sjoreen
Oak Ridge National Laboratory, Oak Ridge, Tennessee 37831
(Received 10 January 1989)

We have determined the ground-state photon decay probability and the branching ratios to a number of low-lying states as a function of excitation energy in ^{208}Pb up to $\sim$15 MeV. Results for the giant quadrupole resonance at 10.6 MeV include determination of a ground-state electromagnetic transition strength $B(E2)\uparrow = 5800 \pm 1600\ e^2\text{fm}^4$ and observation of strong suppression of the $E1$ transition from the resonance to the 3^- state at 2.6 MeV. These results confirm the common assumption of the predominately isoscalar character of the 10.6-MeV resonance. Ground-state gamma coincidences enable us to isolate the isovector giant dipole resonance, which is too weak to be seen in singles, and to test models for its excitation in heavy-ion scattering.

I. INTRODUCTION

The giant electric multipole resonances (GR) are simple collective states, which are strongly excited by the inelastic scattering of hadronic probes.[1,2] The coherent GR state may decay directly by emission of particles or photons, or it may be damped (mixed) into the dense spectrum of more complex states.[3-6] The former process is characterized by a width $\Gamma^\uparrow$, referred to as the escape width, while the damping is characterized by $\Gamma^\downarrow$, the spreading width. For a heavy nucleus, $\Gamma^\downarrow/\Gamma$ (where $\Gamma = \Gamma^\uparrow + \Gamma^\downarrow$) is generally estimated to be ~ 0.9.[3,5,6]

Coincidence experiments[5-8] designed to investigate decay properties now make up a significant part of the experimental study of giant resonances. Since most giant resonances lie above the particle emission threshold the dominant decay mode is usually nucleon or alpha emission (neutron emission in heavy nuclei) with photon decay having a small ($\lesssim 10^{-3}$) probability. Nucleon emission can in principle carry important information about the microscopic structure of resonances, damping mechanisms and damping rates. Photon decay studies face difficulties resulting from the small probability of such events, yet they too can provide significant information, illuminating aspects of the GR different than those probed by nucleon decays.

Photon decay data can be extremely sensitive to GR multipolarity. For example, photon decay back to the ground state following heavy ion inelastic scattering is almost certain to be dominated by the isovector giant dipole resonance (IVGDR). Under very favorable conditions ground-state decay of the giant quadrupole resonance (GQR) might also be observed. In the 10 to 25 MeV region of excitation energy higher multipolarities are extremely unlikely to contribute to the g.s. decay. This is illustrated in Fig. 1, which shows the ground-state photon width ($\Gamma_{\gamma 0}$) expected for a sharp state exhausting 100% of the respective isoscalar (IS) or isovector (IV) energy weighted sum rule (EWSR) as a function of multipolarity and energy, relative to that for the GDR. Ground-state photon decay can also yield data on the electromagnetic strength of resonances, and can provide simple, well-defined conditions under which we can investigate the multistep theory of nuclear reactions in terms of which GR decay is conventionally discussed.

Photon decays from the GR to low-lying excited states are also potential sources of significant information. These data, like ground-state decays, provide significant multipole selectivity—but are not limited to $L=1$ and 2 resonances. Decays to excited states, like ground-state decay, are dominated by $E1$ transitions. Thus, for example, transitions from the GR region to a low-lying 5^- state in an even-even nucleus is clear evidence for high-spin (4^+ or 6^+) strength. Decays to low-lying collective states can provide important information about the coupling of GR modes to low-frequency collective modes. Recent calculations[9,10] have shown that $E1$ transitions between isoscalar GR and low-lying isoscalar collective states can be strongly suppressed. Thus, study of such transitions can provide important data on the isospin character of resonances.

II. EXPERIMENT AND DATA REDUCTION

In this paper we report on experiments carried out using the coupled accelerators at the ORNL HHIRF to study the photon decay of the giant resonance region ($\sim$9 to 15 MeV of excitation) in ^{208}Pb. The resonances were excited by inelastic scattering of 381 MeV ^{17}O. This projectile was chosen because the low neutron binding energy (4.1 MeV) minimizes interference due to gamma rays from projectile excitation. The self-supporting target was 2 mg/cm^2 of ^{208}Pb, enriched to $>99\%$. The scattered ^{17}O ions were detected in six cooled Si surface barrier detector telescopes arranged symmetrically around the beam at an angle $\theta = 13°$, each subtending $\Delta\theta = \pm 1.5°$ and $\Delta\phi = 9°$, respectively, for a total solid angle of 22.6 msr. The telescopes consisted of two elements of thickness $\sim$500 and $\sim$1000 μm, respectively. The energy

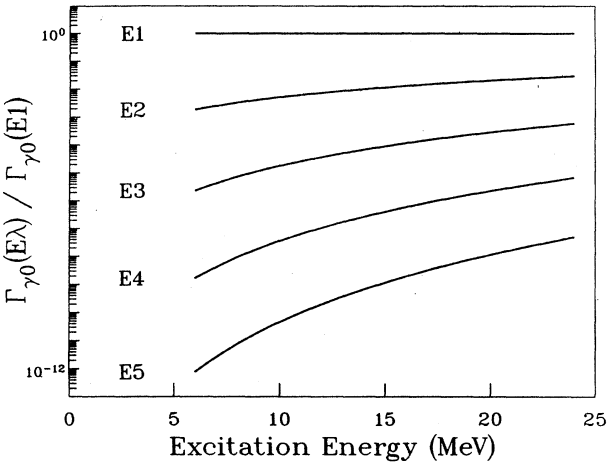

FIG. 1. Ground-state gamma widths of hypothetical sharp states fully exhausting the appropriate isovector or isoscalar energy weighted sum rule as a function of the excitation energy of the state, relative to the $E1$ width.

resolution ranged from ~800 to 950 keV in the various runs. A mass resolution sufficient to clearly separate ^{17}O from neighboring isotopes was achieved. A singles spectrum of inelastically scattered ^{17}O is shown in Fig. 2. Strong excitation of the giant resonance region centered at ~11 MeV is evident. Excitation of the 4.085 MeV 2^+ state dominates the low-energy region. The energy region below ~2.6 MeV (near the peak of the 2.61 MeV 3^- state) was scaled down during data acquisition by factors ranging from 512 to 64.

Decay products were detected in 70 elements of the

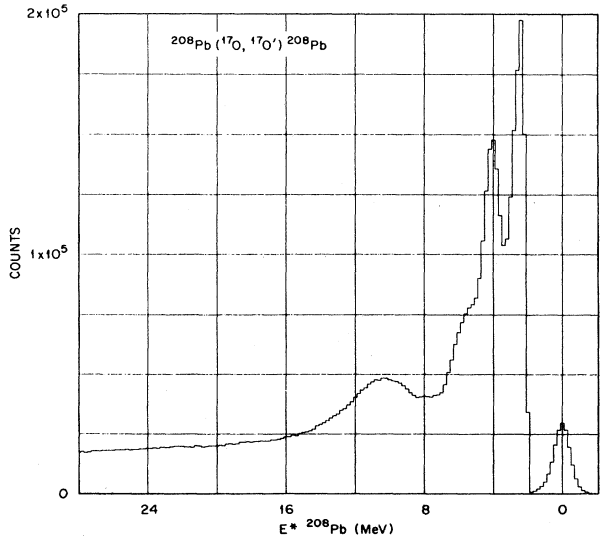

FIG. 2. Spectrum of 380-MeV ^{17}O scattered by ^{208}Pb at $\theta_{lab}=13°\pm1.5°$. The elastic peak has been prescaled by a factor of 512. The large bump between 9 and 15 MeV results from excitation of giant resonances.

ORNL spin spectrometer. The spectrometer, which has been described in detail elsewhere,[11] consists of 72 independent NaI modules which together form an almost spherical shell surrounding the target chamber. The modules at 0° and 180° were removed to allow the beam to enter and leave the chamber. The response of the spectrometer to high-energy photons was determined using the $^{12}C(p,p'\gamma)^{12}C$ reaction with 24 MeV protons, which produces 4.4, 12.7, and 15.1 MeV photons, and the $^{16}O(p,p'\gamma)^{18}O$ reaction at the same bombarding energy which produces 6.13 MeV photons. The response at lower energy was obtained from a variety of radioactive sources.

The very large efficiency and multiple elements of the spin spectrometer make it an excellent tool for photon decay studies of GR. The chief experimental problems were, first, isolating photon decays from the $>10^3$ times more frequent neutron decays encountered in the GR region; second, distinguishing direct photon transitions to the ground state from multiple or cascade decays; and third, isolating decays which directly populated low-lying states of interest (e.g., the 3^-, 2.61-MeV state) by a single photon from the GR region.

The raw data obtained from the spin spectrometer consisted of pulse heights from the individual NaI elements and times of these pulses relative to the inelastically scattered ^{17}O with which they were in coincidence. A number of derived parameters were obtained which were used to address the experimental problems raised in the preceding paragraph. The total pulse height, $H=\Sigma h_i$, was constructed by summing all those NaI pulses which occurred within a prompt time window. This window (which was a function of pulse height) was narrow enough to eliminate pulses resulting from detection of neutrons with energies less than ~5 MeV, due to their longer flight time to the NaI. Single high-energy photons are extremely unlikely to trigger a single NaI detector. Consequently, the number of individual detectors triggered is not very useful for isolating single photons. A more useful quantity can be constructed by considering each pulse height observed in an element of the spectrometer as a vector quantity, $\mathbf{h}_i$, with direction determined by the location of the element, from which the quantity $V=|\Sigma \mathbf{h}_i|/H$ is formed. For a single high-energy gamma ray, $V\sim1$, while for multiple gamma rays a smaller value of V is much more likely. Other useful quantities are the cluster sum pulse height and the cluster multiplicity. They are constructed for each event as follows. First, the largest pulse height is found, and a cluster sum is created by adding to it all the pulse heights in the five or six nearest neighboring detectors. Then the next largest pulse height not yet included in a sum is found, and a cluster sum is calculated from its nearest neighbors (not including those already used). This process continues until all the NaI pulses which satisfy the time gate are used. The number of clusters found is called the cluster multiplicity. For events such as those encountered in ^{208}Pb decay, in which a small number of gamma rays (usually fewer than four) are emitted, the cluster sums are a much better reflection of individual photon energies than the separate NaI pulse heights.

The separation of neutron decays from purely gamma decays is illustrated in Fig. 3. The horizontal axis shows excitation energy in ^{208}Pb obtained from the kinetic energy of the inelastically scattered ^{17}O ions. The vertical axis is the sum photon energy. The solid line starting near zero on the horizontal axis in the figure is the line which would be occupied by events for which these two quantities are equal. Another line is drawn 7.4 MeV (the neutron separation energy in ^{208}Pb) below this line in Fig. 3. Events in which a neutron was emitted should lie below this line in the figure. Pure photon decays were isolated by placing a gate around the equal energy line (the width of the gate in each direction reflects instrumental resolution).

These procedures effectively discriminate against neutrons originating from the targetlike nucleus. In addition a significant yield of large pulse height, short flight time, events, presumed to arise from neutrons and protons emitted sequentially from the projectilelike nucleus following ^{208}Pb(^{17}O,^{18}O*) and ^{208}Pb(^{17}O,^{18}F*) reactions, respectively, was observed. Such events were found to be confined to small angles ($\lesssim 40°$) with respect to the direction of emission of the ^{17}O ejectile. This tight correlation with the ^{17}O direction, provides an essentially complete discrimination against such events. In the analysis, ground-state photon decay events in which the largest pulse height was detected within 60° of the ejectile direction were eliminated to guard against contamination from these sequential decays.

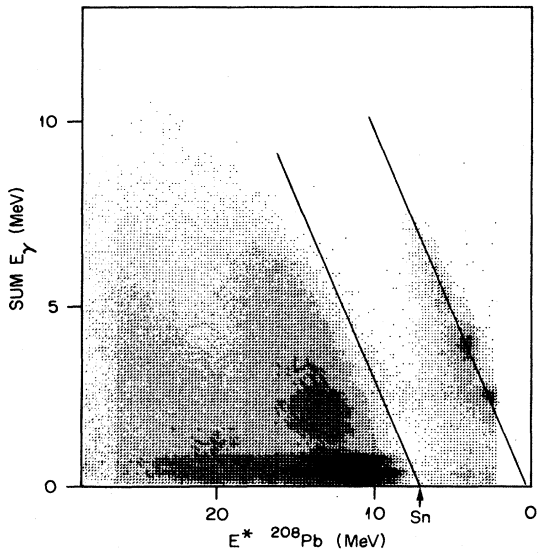

FIG. 3. Two-parameter density plot of events from ^{208}Pb(^{17}O,^{17}O′) in which one or more NaI detectors registered a delayed pulse. The abscissa is derived from the energy lost by the inelastic ^{17}O. The ordinate is the sum of the γ-ray energies seen in the NaI detectors. The locus of equal energies ($E^* = \Sigma E_\gamma$) is indicated by a line on the plot passing through $E^* = 0$. Another line is drawn parallel to the equal energy line, offset down by the neutron separation energy ($S_n = 7.4$ MeV) in ^{208}Pb on the sum E_γ axis. Events in which a neutron is emitted should all lie below and to the left of this latter line.

Direct transitions to the ground state were isolated by requiring that the cluster multiplicity be one and the parameter $V \geq 0.98$. [This value was determined empirically using the ^{12}C(p,p') calibration data.] This is illustrated in Fig. 4. The region in which ground-state gamma decay events are expected to lie is between the pair of lines on the figures. Figure 4(a) was generated with no condition on the V parameter ($V \geq 0$). Figure 4(b) shows the result of imposing the $V > 0.98$ condition. Figure 5 shows spectra obtained by projecting the gates in Figs. 4(a) and 4(b) onto the sum photon-energy axis. Taking the ratio

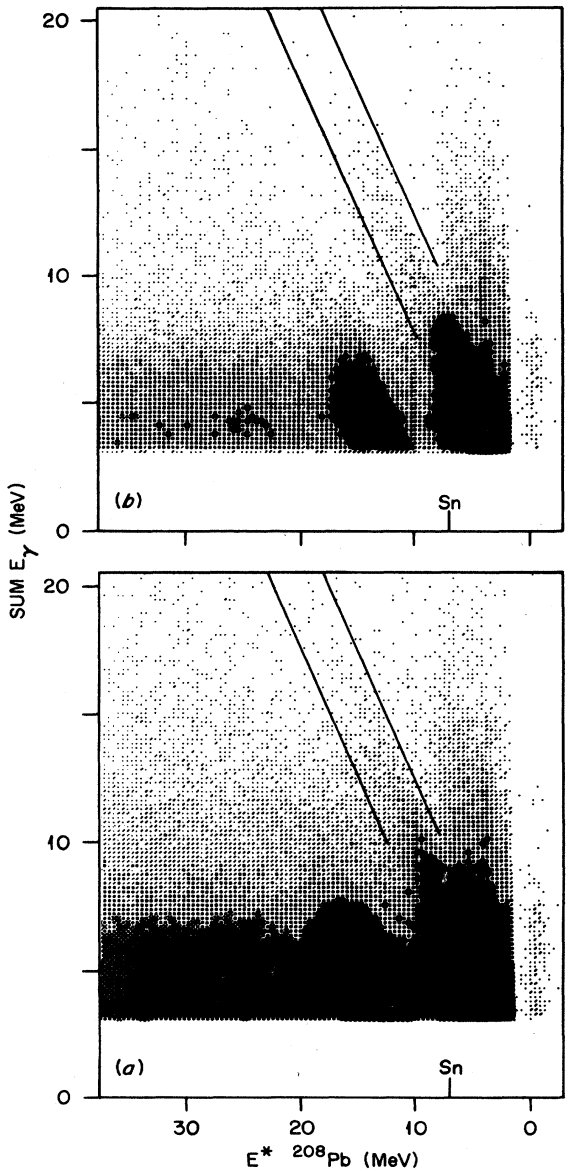

FIG. 4. Two-parameter density plot of events from ^{208}Pb(^{17}O,^{17}O′) in which no NaI detector registered a delayed pulse. The axes are the same as for Fig. 3. Events falling between the pairs of lines are due to γ-decay events: (a) all events ($V > 0$); (b) events satisfying the additional requirement $V > 0.98$ to select ground-state transitions.

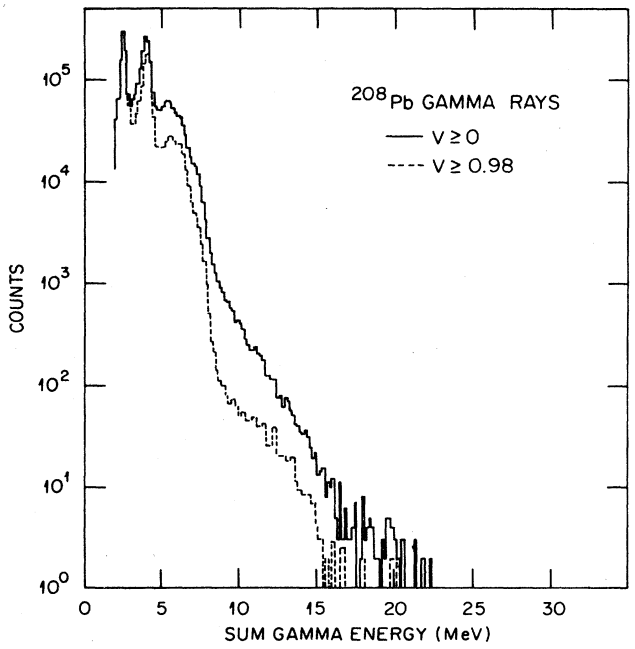

FIG. 5. Gamma-ray spectra from ^{208}Pb for $V \geq 0.98$ (only ground-state gamma rays), and $V \geq 0$ (all gamma rays).

of spectra such as these produces the ground-state branching spectrum shown in Fig. 6(a). The peaks in this spectrum below the neutron binding energy are at the position of states in ^{208}Pb known to have large ground-state branches. Above the neutron binding energy, the ground-state branching falls off rapidly until the vicinity of the giant quadrupole resonance (GQR) is reached. The large peak in the branching spectrum between ~9 and 15 MeV nicely illustrates the strong localization of electromagnetic strength to the ground state in this region. The bump contains contributions from both the GQR at 10.6 MeV and the giant dipole resonance (GDR) at 13.4 MeV, which is very weakly excited in the reaction.

The angular correlations of ground-state gamma radiation for two energy windows, intended to emphasize the GQR and GDR is shown in Fig. 7. The angles are defined with respect to the z axis along the direction of the recoiling ^{208}Pb nucleus. The correlations are integrated over ϕ in this coordinate system. Calibration for the complex angular efficiency resulting from the elimination of events near the direction of the ejectile emission and the absence of NaI detectors at 0° and 180° was accomplished by means of Monte Carlo simulation. The results were checked with the angular correlation of decays from the 2^+, 4.08 MeV and 3^-, 2.61 MeV states. The dashed-dotted line in Fig. 7 is obtained from a DWBA calculation assuming excitation of a 2^+ state at 10.6 MeV and followed by an $E2$ ground-state decay. The dotted line is a similar calculation for the 1^- IVGDR, assumed to be centered at 13.4 MeV. Clearly the angular correlation in the higher-energy bin is consistent with pure $E1$ emission while that for the lower bin requires a large contribution from $E2$ transitions. From the angular correlation, we deduce an $E2$ contribution in the lower-energy bin of $46 \pm 18\%$ (assuming only $E2$ and $E1$ contribute). The heavy solid line will be discussed along with a more quantitative analysis of the ground-state photon decay yield in a later section.

The experimental techniques outlined in this section also make it possible to isolate cascade decays through low-lying excited states as a function of excitation energy. This analysis was carried out in two ways, one to provide a qualitative picture of the relative strength of particular cascade decays as a function of excitation energy, and the

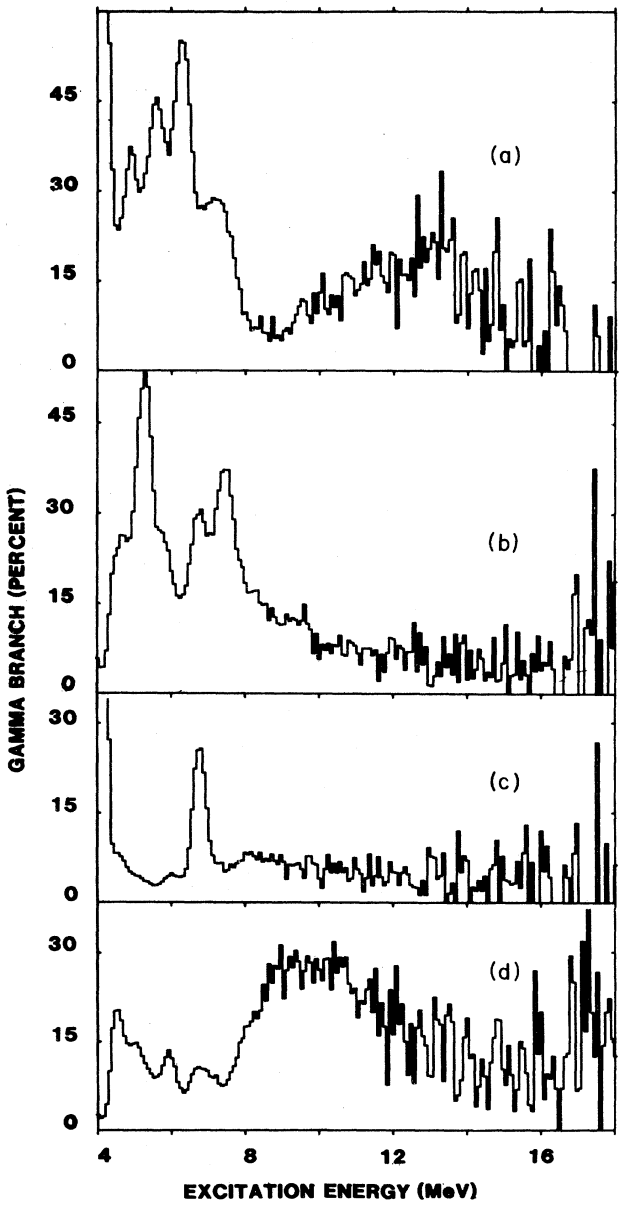

FIG. 6. Relative gamma-decay strengths for transitions to a number of low-lying levels in ^{207}Pb: (a) for ground-state decays; (b) for transitions to the 2.61-MeV, 3^- state; (c) the 4.08-MeV, 2^+ state; (d) the 4.97-MeV, 3^- state.

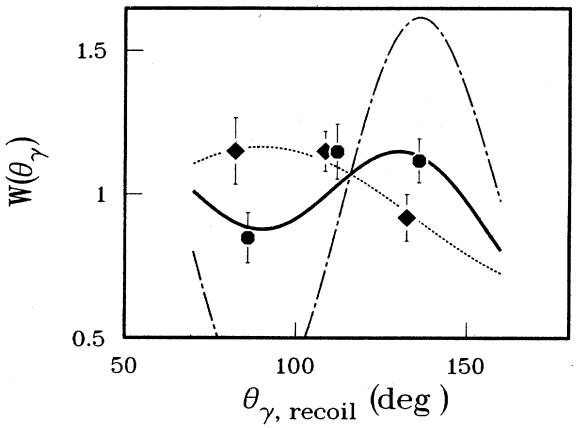

FIG. 7. Experimental γ_0 angular correlation for excitation energy bins 9–11 MeV (circles) and 12–15 MeV (diamonds). The dashed curve is the DWBA prediction for pure $E1$ decay from a 1^- state. The dashed-dotted curve is for pure $E2$ decay from a 2^+ state. The solid curve represents the $E2+E1$ mixture predicted for the 9–11 MeV region by the calculations discussed in Sec. I and shown in Fig. 11.

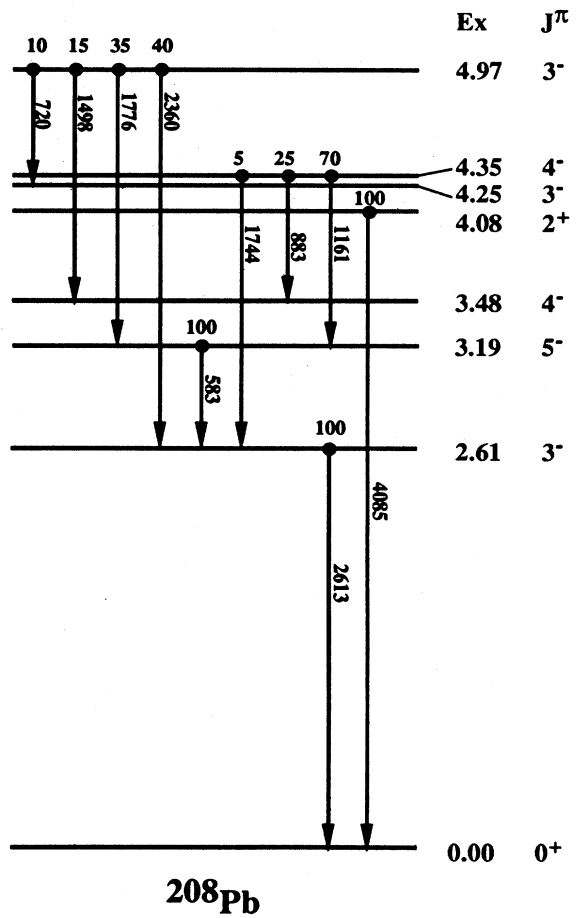

FIG. 8. A selected subset of low-lying levels of ^{208}Pb which are relevant to the present study, along with their photon decay branches. (From Ref. 12.) Level energies (MeV) and spins are given to the right of each level. Vertical lines represent gamma decays and are labeled by energy (keV) and branch (%).

other to provide more quantitative information on the photon branches from an excitation energy region spanning the peak of the 10.6 MeV GQR. A level scheme[12] of selected low-lying states in ^{208}Pb is given in Fig. 8, showing gamma decay properties relevant to the analysis.

The qualitative distributions of relative branching strength were obtained by generating excitation energy spectra subject to the following requirements: (1) the total photon energy equals the excitation energy (within detector resolution), (2) a gate on photon cluster sum energy (defined above) corresponds to the energy of a known deexcitation gamma-ray from the low-lying state in question, and (3) a condition on the cluster multiplicity which depended on the particular case and is discussed below. Samples of such spectra are shown in parts (b), (c), and (d) of Fig. 6. Figures 6(b) and 6(c) are for decays to the 2.6 MeV, 3^- state and 4.08 MeV, 2^+ state, respectively. Because both of these states themselves decay 100% to the ground state, it is possible to separate events which corresponds to direct population of these states from multistep cascades via intermediate states by requiring that the cluster multiplicity be 2. Figure 6(d) corresponds to cascades passing through the 4.97 MeV, 3^- state, which has a more complex decay scheme,[12] which makes it more difficult to eliminate cascades via an intermediate state. The plot in Fig. 6(d) was generated with a gate on photon energy at 1.78 MeV, which corresponds to a gamma ray known to depopulate the 4.97 MeV state,[12] and a requirement that the cluster multiplicity be three or four. The vertical scale is corrected for the fact that the 1.78 MeV photon is a 35% branch for the 4.97 MeV state, as shown in Fig. 8. The 4.97 MeV state is not uniquely identified by the gate at 1.78 MeV. A small contribution from the 4.36 MeV state through its small (4%) 1.74 MeV decay is possible. A more quantitative study of the gamma decay branching from broad excitation energy regions was obtained by generating individual photon cluster sum energy spectra for various cluster multiplicities subject to gates on excitation energy and total gamma sum energy. Individual peaks were identified and associated with known energy levels in ^{208}Pb using data from Ref. 12. Branching ratios were obtained from fits to these peaks, and the adopted level scheme of Ref. 12. Analysis of spectra generated for an excitation energy gate from 9.5 to 11.5 MeV confirm the 4.97 MeV state as the primary source of the $\sim$1.78 MeV photons used as a gate in generating Fig. 6(d). If we accept the level scheme and decay branches of Ref. 12, a significant contribution from the 4.36 MeV state can be ruled out.

III. SUM RULES AND GAMMA WIDTHS

The deformed optical potential model, applied in the DWBA is a standard tool for studying the inelastic excitation of collective states. For completeness we summarize here the basic relations used in this work, following the notation and philosophy of Ref. 13.

All DWBA calculations reported in this work were performed with the code Ptolemy,[14] using in all cases the standard Coulomb transition potential provided by the code. For excitations with $L \geq 2$ a nuclear transition po-

tential with the radial form[13]

$$G_l(r)=\beta_l R\frac{dU(r)}{dr} \tag{1}$$

was used, where $U(r)$ is the optical potential and the strength of the excitation is given by the deformation length βR. The strength of collective states is conventionally expressed as a fraction of the energy weighted sum rule (EWSR), which for $l\geq 2$ can be written[13] in terms of $\beta_l R$ as

$$(\beta_l R)^2=l(2l+1)\frac{2\pi\hbar^2}{3AmE}\ , \tag{2}$$

where A is the mass number of the excited nucleus, m is the nucleon mass, and E is the energy of the state.

For $l=0$ excitations the radial form of the transition potential used was[13]

$$G_0(r)=-\alpha_0\left[\frac{C}{R}\right]\left[3U(r)+r\frac{dU(r)}{dr}\right], \tag{3}$$

where C is the half-density radius of the excited nucleus and R is the radius of the optical potential. The EWSR for $l=0$ can be expressed[15] as

$$\begin{aligned}&\alpha_0^2=2\pi(\hbar^2/m)(A\langle r^2\rangle E)^{-1}\ ,\\ &\langle r^K\rangle=\int_0^\infty r^{K+2}\rho(r)dr\Big/\int_0^\infty r^2\rho(r)dr\ ,\end{aligned} \tag{4}$$

where $\rho(r)$ is the density distribution of the excited nucleus. If $\rho(r)$ is approximated by a Fermi function with half-density radius C and diffuseness parameter a, then

$$\langle r^K\rangle=\frac{3}{K+3}\left[C+\frac{\pi^2a^2(K+5)}{6C}\right]^K.$$

Excitation of the isovector giant dipole resonance (IVGDR) by hadronic probes has been discussed at length in Ref. 13. For ^{17}O scattering at 22 MeV per nucleon Coulomb excitation already dominates GDR excitation. The strength of the excitation is defined by the electromagnetic reduced matrix element $B(E1)\uparrow$. The classical EWSR for $E1$ excitation of a nucleus with N neutrons and Z protons is[15]

$$B(E1)=\left[\frac{9\hbar^2}{2\pi m}\right]\frac{NZ}{EA}\ e^2\mathrm{fm}^2\ . \tag{5}$$

For an isoscalar projectile the nuclear part of the transition potential can be written as[13]

$$G_1(r)=-\frac{2\alpha_1}{A}\left[Z\frac{dU_n}{dr}-N\frac{dU_p}{dr}\right], \tag{6}$$

where the classical $E1$ sum rule gives

$$\alpha_1=\frac{\pi\hbar^2}{2m}\frac{A}{NZE}\ . \tag{7}$$

U_n and U_p are the neutron and proton parts of the optical potential, where $U=U_n+U_p$, and based on the philosophy of the folding model, U_n and U_p are assumed to reflect the neutron and proton densities, ρ_n and ρ_p, of the excited nucleus. In applying Eq. (6) we obtain the radii R_n and R_p of the potentials U_n and U_p from the experimental data for C_n and C_p (half-density radii) of the neutron and proton distributions by assuming $\Delta R=R_n-R_p\approx C_n-C_p$ and relating R_n and R_p to the radius of U by $R\simeq(ZR_p+NR_n)/A$. If $\rho_n/\rho_p=N/Z$ for all r, $G_1(r)=0$. Otherwise it is finite. We neglect, at this point, the effect of the excess neutron in ^{17}O.

Macroscopic descriptions of giant multipole resonances in nuclei, classify oscillations as "isovector" or "isoscalar" according to whether the neutron and proton excitations are out-of-phase or in-phase, respectively. A pure isovector or isoscalar excitation would have neutron and proton matrix elements equal in magnitude ($|M_N|=|M_p|$). In macroscopic pictures of giant resonances it is generally assumed instead that the neutron and proton deformations are equal, i.e., $\beta_l(n)\sim\beta_l(p)$ which implies[13] $|M_n/M_p|\sim N/Z$. With this assumption EWSR limits for the electromagnetic reduced transition probabilities associated with giant resonances for $L\geq 2$ can be obtained directly from the expressions for $(\beta R)^2$ given earlier[15] and the scaling $(\beta_l R)^2=[\beta_l(p)R_p]^2$

$$B(El)\uparrow=|3Z\beta_l(p)R_p^l/4\pi|^2e^2=|M_p|^2e^2\ . \tag{8}$$

In these expressions it is assumed that the matter and charge distributions can be represented by uniform distributions of radius R and R_p, respectively. The corresponding ground-state gamma decay widths for a single state at energy E is (for any l)[15]

$$\Gamma_{\gamma 0}=\frac{8\pi(l+1)}{l[(2l+1)!!]^2}\left[\frac{E}{\hbar c}\right]^{2l+1}g_I B(El)\uparrow\ , \tag{9}$$

where $g_I=(2I_0+1)/(2I_R+1)$. I_0 and I_R are the spins of the resonance state and ground state, respectively. By analogy with Eq. (8) we can write an expression for the mass reduced transition probability $B(l)\uparrow=(M_n+M_p)^2$ by replacing Z by A and R_p and β_p by R and β. Satchler has stressed that the quantity determined by a collective model analysis of inelastic scattering is the deformation length $\beta_l R$. We thus use an expression for $B(l)\uparrow$ (e.g., 14.70b of Ref. 13) which, is expressed explicitly in terms of the deformation length ($l\geq 2$)

$$B(l)\uparrow=(\beta_l R)^2|(l+2)A\langle r^{l-1}\rangle/4\pi|^2\ , \tag{10}$$

where $\langle r^{l-1}\rangle$ is a radial moment of the density distribution of the excited nucleus, defined as in 4 above.

For states with $L\geq 2$, simultaneous determination of the electromagnetic reduced matrix element, and the strength of the hadronic excitation enables one to infer the ratio of neutron to proton excitation matrix elements, and hence is sensitive to the isospin character of the resonance. Since the $B(l)$ is proportional to $|M_n+M_p|^2$ while $B(El)$ is proportional to $|M_p|^2$, we obtain

$$\left|\frac{M_n}{M_p}\right|=\left[\frac{B(l)}{B(El)}\right]^{1/2}-1\ . \tag{11}$$

IV. SINGLES ANALYSIS

The inelastic singles data in the present experiment were acquired at a single scattering angle, with relatively

poor energy resolution. Consequently, an analysis which attempts an *ab initio* decomposition of the giant resonance region into peaks corresponding to different multipolarities is not sensible. We instead assume peak positions and widths shown in Table I from the high-resolution ^{208}Pb(p,p') data of Ref. 16 and fit only the peak intensities.

A singles spectrum of inelastic ^{17}O scattering on ^{208}Pb was shown in Fig. 2. A similar spectrum, with the elastic region suppressed, is reproduced in Fig. 9(a). Two possible estimates of the continuum underlying the GR peaks are shown as dotted (#1) and solid (#2) lines. Both curves were obtained from a quadratic polynomial fit to the region from 22 to 38 MeV extrapolated to lower energy, modified by a factor of the form $(1+e^{-(E-E')/\Delta})^{-1}$ to account for the decrease in level density and consequent decline in continuum excitation at low energy. Background #2 (solid) in Fig. 8(a) corresponds to $E'=6$ MeV and $\Delta=2$ MeV while the background #1 (dotted) corresponds to $E'=10$ MeV, $\Delta=3$ MeV. The solid background is very similar above ~ 9 MeV, to those which have been used in previous analyses of GR singles (see e.g., Refs. 16 and 17), and in fact will be seen to produce resonance strengths in close agreement with those of Ref. 16. Since, however, there is some arbitrariness in this curve, the results of a complete analysis of the singles data are included using the dotted curve on Fig. 9(a) which we regard as a reasonable lower limit to the continuum contribution in the vicinity of 10 MeV. Figures 9(b) and 9(c) show the data of Fig. 9(a) after subtraction of these two background estimates, together with the results of fitting the spectra with the set of peaks obtained from Ref. 16 (listed in Table I). The complete spectrum down to the cutoff at 2.3 MeV was fitted simultaneously by including a selected set of bound states taken from Ref. 12. Of these only the result for the well resolved and strongly excited 2^+, 4.08 MeV state is relevant to the GR results, since it was used to establish an overall normalization, based on an excitation cross section calculated in the DWBA using a strength $\beta R = 0.466$.[12] This normalization agreed with one based on target thickness and beam current integration with in the accuracy ($\sim 20\%$) to which these quantities are known.

The optical potential used for all DWBA calculations in the paper, was taken from Ref. 17 and consisted of real and imaginary parts of Woods-Saxon form with

$$V_0 = 60 \text{ MeV}, \quad W = 30 \text{ MeV},$$

$$r = r_i = 1.17 \text{ and } a = a_i = 0.67 .$$

Sum rule strengths and transition potentials were calculated using the expressions in Sec. III, with the density distributions of matter protons and neutrons in ^{208}Pb assumed to be described by Fermi functions with parameters[13] $C=6.70$, $C_n=6.80$, $C_p=6.54$, and $a=a_n=a_p=0.545$.

The cross sections obtained from the fits in Fig. 9 are shown in Table II along with corresponding strengths expressed in terms of the fraction of the corresponding energy weighted sum rule (EWSR) exhausted. The strengths obtained in (p,p') are given in Table I. Note

TABLE I. Levels from ^{208}Pb(p,p') (Ref. 13) used for the singles analysis (Fig. 8).

Excitation energy (MeV)	L	FWHM[a] (Ref. 13) (MeV)	EWSR fraction (%)
7.36	2	0.4	6.5
7.84	2	0.4	4.2
8.11	4	0.4	3
8.35	3	0.4	4
8.86	2	0.4	7
9.34	2	0.4	5
10.6	2	2.0	70
12.0	4	2.4	100
13.9	0	2.9	100

[a]Full width at half maximum. In the present analysis widths were fixed at the values in this table added in quadrative to the experimental resolution of 950 keV.

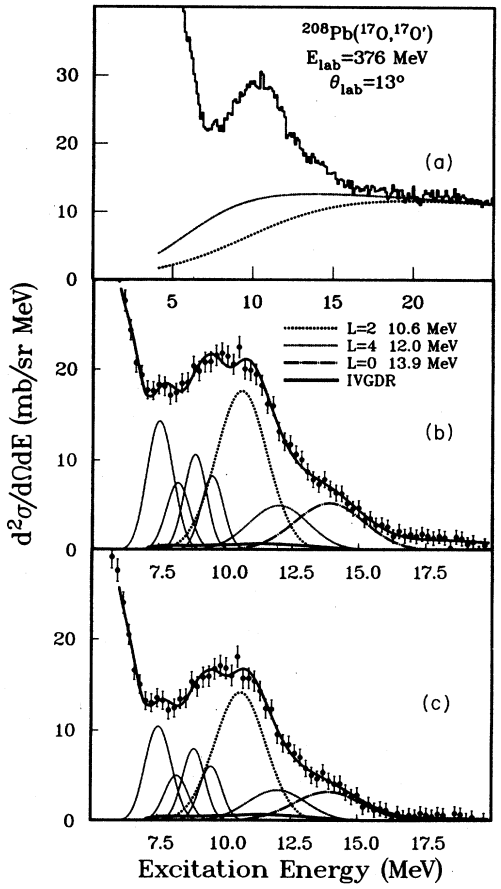

FIG. 9. Analysis of inelastic singles spectrum. (a) shows the singles spectrum together with two possible estimates of the continuum underlying the GR region as discussed in the text. (b) and (c) show the spectrum in the GR region after subtraction of the dotted and solid backgrounds, respectively, together with fits to the data employing the set of peaks and peak properties given in Table I (Ref. 16). The resulting cross sections are given in Table II.

TABLE II. Fit results.

E^*	L	Cross section (mb/sr) 13°±1.5° Background #1	Background #2	EWSR fraction Background #1	Background #2
4.085	2	68.3	68.3		
7.36+7.84	2	17.4 (1.0)	12.6 (1.8)	15	11
8.11+8.35	(4+3)	8.1 (0.98)	5.4 (0.9)	4	2
8.8	2	11.1 (1.5)	8.2 (1.5)	13	10
9.4	2	8.6 (1.5)	6.2 (1.5)	12	9
10.6	2	42.2 (2.0)	33.9 (2.1)	98	78
12.0	4	13.7 (2.1)	9.4 (1.8)	18	13
13.9	0	17.0 (2.6)	10.5 (1.5)	133	83

that two pairs of peaks, which are unresolved in the present data were each fit as a single peak made up of two Gaussians with relative strengths based on the (p,p') results. It can be seen that the $(^{17}O,^{17}O')$ spectrum is well accounted for by the states seen in (p,p'), and that the excitation strengths obtained with background #2 [Fig. 8(c) and Table II], agree very well with those from Ref. 16 (Table I). The set of results with background #1, which gives larger strengths than the (p,p') analysis, is included to illustrate the magnitude of uncertainty introduced by the background subtraction. The excitation strengths were obtained from the ratio of the observed cross section to that calculated in the DWBA for a strength corresponding to a state with the full EWSR located at the centroid of the peak.

The broad very weak structure shown as a solid line in Figs. 9(a) and 9(b) stretching from ~7.5 to ~15 MeV corresponds to the IVGDR. It is not included in the results in Table II. Its strength was not allowed to vary in the fits. Even though it is essentially irrelevant in the singles analysis, it warrants further consideration because of its importance in the ground-state gamma decay. The IVGDR line shape and cross section shown in Fig. 9 were calculated from an experimental strength distribution based on the photonuclear cross section[18] shown in Fig. 10 (heavy solid line) using

$$\frac{d^2\sigma}{d\Omega dE} = b_{E1}(E)\left[\frac{d\sigma}{d\Omega}\right]_{b=1},$$

where $b_{E1}(E)$ is the distribution of $E1$ reduced transition probability obtained from the photonuclear cross section[15] $[b_{E1}(E)=(9\hbar c/16\pi^3)\sigma(E)/E\ e^2\text{fm}^2/\text{MeV}$, where $\sigma(E)$ is photonuclear cross section in $\text{fm}^2]$, and $(d\sigma/d\Omega)_{b=1}$ is the DWBA cross section for a unit $E1$ strength calculated on a 1 MeV grid from 6 to 25 MeV and interpolated. The corresponding cross section distribution is shown as a heavy dashed line in Fig. 10. The excitation of the IVGDR in ^{17}O scattering is dominated, even at 376 MeV, by Coulomb excitation. This is responsible for the strong energy dependence of the excitation which, along with the large width of the $E1$ resonance, results in a cross section distribution significantly different from the photonuclear cross section. The nuclear excitation transition potential used in the calculation was discussed in Sec. III. The total IVGDR cross section, integrated from 7.4 to 25 meV was calculated to be 5.6 mb/sr.

The analysis of the singles data is completely insensitive to the presence or absence of the IVGDR, and to its excitation distribution. The coincidence with photons connecting the GR directly with the ground state changes this completely. We note in passing that *all* broad resonance states should be treated in the way we treat the IVGDR to properly relate the cross section distribution observed with a particular probe to the resonance strength distribution. In practice the difference between the shape of cross section and strength distributions is very small for the other resonance states ($L=2$, 4, and 0) considered here.

V. GROUND-STATE GAMMA DECAY

In order to deal quantitatively with ground-state photon coincidence data we must consider how to relate the coincidence cross section to the inelastic scattering cross

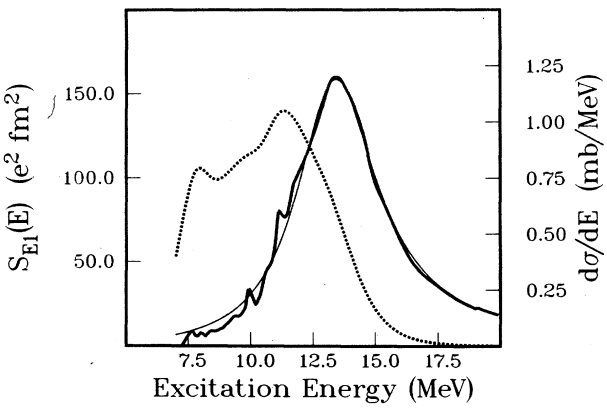

FIG. 10. GDR strength and excitation distributions. The heavy solid line shows the experimental photonuclear cross section for ^{208}Pb reported in Ref. 18, which we assume to reflect the IVGDR strength function. The light solid line is a Lorentz function fit to these data ($E_0=13.42$, $\Gamma=3.95$, $\gamma_0=4b$). The heavy dashed line is the predicted distribution of excitation cross section for the $^{208}Pb(^{17}O,^{17}O')$ reaction at 378 MeV and $\theta_{lab}=13°$, corresponding to the strength function deduced from the photonuclear cross section.

section and the resonance strengths.

The absolute yield of ground-state photons can be calculated from the properties of a giant resonance by applying the ideas of the multistep theory of nuclear reactions.[19] The collective $1p$-$1h$ GR state is considered as a doorway state which couples strongly to the inelastic scattering process. This state damps into the more complex $2p$-$2h$, $3p$-$3h$, etc. states eventually reaching the fully damped compound states. According to the multistep compound (MSC) model of Ref. 19, the cross section for a given emission process can be written as an incoherent sum over these various stages. The cross section for emission of ground-state photons following inelastic excitation can be expressed as

$$\sigma_{x,x'\gamma_0}(E)=\sigma_{x,x'}(E)\left[\sum_{i=1}^{r}\frac{\Gamma_{\gamma 0,i}}{\Gamma_i}\left[\prod_{j=1}^{i-1}\frac{\Gamma_j^{\downarrow}}{\Gamma_j}\right]\right], \quad (12)$$

where $\sigma_{x,x'}(E)$ is the distribution of excitation cross section obtained from the giant resonance strength distribution and a DWBA calculation as discussed for the IVGDR in the previous section. The sum in parentheses in Eq. (12) runs over the hierarchy of levels of complexity from the doorway stage ($i=1$) to the compound (rth) stage. The quantity in brackets is the so-called depletion factor which represents the loss due to emission from all stages prior to the ith. The quantity $\Gamma_i^{\downarrow}$ represents the damping width of the ith stage while Γ_i is the total width. In order to simplify the equations, an abbreviated notation is used in which variables such as the scattering angle of the ejectile (x') and the photon emission angles are suppressed. The $\sigma(E)$ on either side of the equal sign may be considered to represent multiple differential cross sections in these variables with all the dependence of $\sigma_{x,x'\gamma_0}(E)$ on the various angles contained in $\sigma_{x,x'}(E)$. In our particular application $\sigma_{x,x'\gamma_0}(E)$ is a differential cross section evaluated at a single scattering angle ($\theta_{\rm CM}=14°$) and integrated over the gamma emission angles. Application of this expression requires a great deal of knowledge concerning the various widths associated with each stage. In this work we will apply the MSC model in a simplified approximate form. (More rigorous application of similar concepts to this problem has been considered by Dias, Hussein, and Adhikari.[19]) We will replace Eq. (12) by a two-step approximation in which only the first (coherent GR doorway) and last (fully damped compound) stages are considered:

$$\sigma_{x,x'\gamma_0}(E)=\sigma_{x,x'}(E)\left[\frac{\Gamma_{\gamma 0}}{\Gamma}+\left[\frac{\Gamma^{\downarrow}}{\Gamma}\right]B_{\rm CN}(E)\right], \quad (13)$$

where the index 1 for the initial doorway stage has been dropped. $\Gamma_{\gamma 0}$ can be calculated[20,21] directly from the GR strength [see Sec. III, Eq. (10)], Γ is identified with the experimental width of the resonance, and $B_{\rm CN}(E)$ is the compound nucleus branching ratio. The quantity in the inner parentheses assures that only that fraction of systems which survive the damping process ($\Gamma^{\downarrow}$ is the damping width) is included in the compound term. Theoretical and experimental results[3,5,6] for ^{208}Pb indicates the $\Gamma^{\downarrow}\gtrsim 0.9\,\Gamma$, so that this factor can be considered as introducing an uncertainty of up to 10% in the compound contribution (we will set it to 0.9). The compound branching ratio can be calculated from mean γ_0 and total widths obtained from Hauser-Feshbach calculations.

In order to evaluate the compound term we recognize that, in the relevant excitation energy region, the experimental averages over many individual compound states. Thus, the average compound γ_0 yield can be expressed as

$$\sigma_{x,x'}(E)B_{\rm CN}(E)=\left\langle\sigma_{xx'}\frac{\Gamma_{\gamma 0}^{\rm CN}}{\Gamma^{\rm CN}}\right\rangle, \quad (14)$$

where the properties inside the angle brackets on the right refer to individual compound states and the angle brackets imply an averaging over E. $\Gamma_{\gamma 0}^{\rm CN}$ and $\Gamma^{\rm CN}$ are ground-state gamma and total widths, respectively. According to the standard collective model description of GR excitation in the DWBA, the excitation cross section is proportional to the ground-state gamma width $\Gamma_{\gamma 0}$. For a state which is almost exclusively Coulomb excited, this proportionality holds independent of model assumptions. We can take this correlation between the entrance and exit channels into account formally by making the substitution

$$\sigma_{xx'}=\frac{\langle\sigma_{xx'}\rangle}{\langle\Gamma_{\gamma 0}\rangle}\Gamma_{\gamma 0}$$

inside the brackets of Eq. (14), and defining $\langle\sigma_{xx'}\rangle\equiv\sigma_{xx'}(E)$, so that all the correlation effects are absorbed in $B_{\rm CN}(E)$. Thus

$$\sigma_{xx'}(E)B_{\rm CN}(E)=\frac{\sigma_{xx'}(E)}{\langle\Gamma_{\gamma 0}^{\rm CN}\rangle}\left\langle\frac{(\Gamma_{\gamma 0}^{\rm CN})^2}{\Gamma^{\rm CN}}\right\rangle \quad (15)$$

or

$$B_{\rm CN}(E)=\frac{1}{\langle\Gamma_{\gamma 0}^{\rm CN}\rangle}\left\langle\frac{(\Gamma_{\gamma 0}^{\rm CN})^2}{\Gamma^{\rm CN}}\right\rangle$$
$$=C\frac{\langle\Gamma_{\gamma 0}^{\rm CN}\rangle}{\langle\Gamma^{\rm CN}\rangle}.$$

The last expression gives the compound γ_0 branch in terms of a Hauser-Feshback estimate (ratio of mean widths) times a correction factor C. This expression, and the evaluation of C have been discussed extensively in the literature.[22–24] The factor C would be 1 if all partial widths were constant in a given energy interval (no fluctuation from level to level) or if the fluctuations between the γ_0 partial widths and the partial widths which dominate $\Gamma^{\rm CN}$ were completely correlated. It has been shown (see, for example, Ref. 22) that if the form of the distribution of partial widths is specified, C can be obtained directly from quantities which are provided by conventional statistical model calculations: namely, the ratio of average widths $\langle\Gamma_{\gamma 0}\rangle/\langle\Gamma\rangle$ and the number of open channels which contribute to $\langle\Gamma\rangle$. We calculate C under the assumption that the γ_0 partial widths and the neutron partial widths which dominate $\Gamma^{\rm CN}$ are distributed according to independent Porter-Thomas distributions.

The resonance strength, which was assumed to be concentrated on a single sharp doorway state at energy E_R is

distributed over many compound nucleus states in the damping process. The corresponding ground state electromagnetic reduced transition probability $B(El)\uparrow$ (see Sec. III) becomes a distribution of reduced transition probability per unit energy, $b_{E\lambda}(E)$. Resonance strength is assumed to be conserved in the spreading

$$E_R B(El) = \int_0^\infty E b_{El}(E) dE \ .$$

The average ground-state gamma width of a compound state is then

$$\langle \Gamma_{\gamma 0}^{\rm CN} \rangle = \frac{X(l) b_{El}(E) \left[\frac{E_\gamma}{\hbar c} \right]^{2l+1}}{\rho_I(E)} \ , \qquad X(l) = \frac{8\pi(l+1)}{l[(2l+1)!!]^2} \ , \tag{16}$$

where $\rho_I(E)$ is the density of compound states of spin I (the resonance spin) at the energy E.

For the giant dipole resonance $b_{\rm E1}(E)$ can be obtained directly from experimental data:

$$b_{\rm E1}(E) = \frac{9\hbar e^2}{16\pi^3} \sigma(E)/E \ , \tag{17}$$

where $\sigma(E)$ is the photonuclear cross section.

Figure 11(a) shows the experimental ground-state photon decay cross section. This spectrum differs from that in Fig. 6 only in that the energy axis is the excitation energy obtained from the $^{17}O'$ energy rather than the sum photon energy. The curves on Fig. 11(a) are the result of applying Eq. (13), considering only the contribution of the IVGDR, based on the experimental strength distribution shown in Fig. 10. The heavy solid curve in Fig. 11(a) represents the total yield from Eq. (13), while the first (doorway) and second (compound) terms are shown separately as dashed-dotted and short-dashed curves, respectively. The shape of the dashed-dotted curve (doorway) reflects the distribution of excitation cross section, while the compound contribution is suppressed at higher energy due to increase in the total width of compound levels with increasing excitation energy. The experimental IVGDR strength extends down only to the neutron separation energy (7.4 MeV). For the compound term only, the curve in Fig. 11(a) includes the contribution of individual experimental 1^- states[25,12] in the 6.5 to 7.4 MeV excitation region, and 2^+ states[25,12] in the 6.5 to 8 MeV range. All calculations have been folded with the experimental response.

The compound results are based on detailed Hauser-Feshbach calculations. Experimental levels[12] of ^{208}Pb and ^{207}Pb were used up to 5 and 4 MeV, respectively. Above these energies an empirical level density formula,[26] adjusted to fit experimental data was used. The calculation depends very little on the level density formula, since neutron decays to the discrete states of ^{207}Pb dominate over most of the energy range considered. Changing to the level density expression of Dilg, Schantl, Vonach, and Uhl[27] changed the results slightly (~few percent) above 13 MeV of excitation energy. The calculation was somewhat more sensitive to the optical model

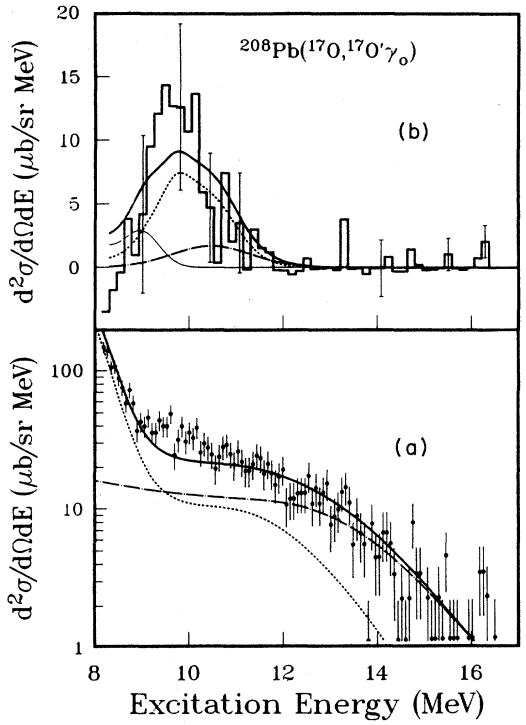

FIG. 11. Ground-state gamma-ray coincidence data compared with calculations using the multistep theory of nuclear reactions, as discussed in the text.

potential used to generate the transmission coefficients. The potential of Rapaport, Kulkarni, and Finlay[28] was adopted, since it was fitted to the ^{207}Pb+n system. Other optical model potentials, including the global $A+n$ potential of Perey and Perey[29] were tried along with a hybrid calculation in which transmission coefficients for low-energy $l=0$, 1, and 2 neutrons were generated from the measured neutron strength function[30] joined to the optical model values above 1 MeV neutron energy. All these different calculations produced variations which differed from the adopted calculation shown in Fig. 11(a) by less than 15%. A single adjustable parameter—an overall scale factor—was used in fitting the calculated IVGDR result to the data of Fig. 11. The fit considered only the region above 12.5 MeV of excitation. The resulting scale factor was 0.85±0.05, which corresponds to an overall GDR strength of 98% of the classical EWSR located in excitation energy region 7.4–25 MeV, compared to 113% found in the same region of the photonuclear data of Fig. 10.

The calculation describes the experimental ground-state photon data very well, except in the region near 10 MeV. This is emphasized in 11(b) in which the difference between the data and the calculated (heavy solid line) spectra of 11(a) is shown as a histogram. The error bars include an estimate of the uncertainty in the subtracted spectrum. The difference spectrum shows a distinct peak located near the energy of the GQR. Since the general considerations discussed in Secs. I and II lead us to expect that only dipole or quadrupole emission will contrib-

ute to this spectrum it is reasonable to associate this excess yield with the GQR. This is consistent with the γ_0 angular correlation data shown in Fig. 7, which shows a pure $E1$ form above 12 MeV but indicates a substantial $E2$ contribution at lower energy.

A calculation identical to that discussed above was therefore carried out for the 10.6 MeV GQR. The dashed-dotted and short dashed curves have the same meaning as in Fig. 11(a). The light solid line shows the contribution of the 8.8 and 9.4 MeV 2^+ peaks (see Table I) to the compound calculation cross sections. The relative strengths of the 8.8+9.4 and 10.6 MeV components were fixed at the value obtained from Table I. Note that in contrast to the dipole case, the $E2$ γ_0 yield is dominated by the compound term in Eq. (13). The heavy solid line in Fig. 11(b) is the total calculated γ_0 yield assuming 100% of the EWSR strength in the 8.8, 9.4, and 10.6 MeV peaks combined. Clearly it describes the histogram fairly well. The total integral from 8 to 13 MeV of the γ_0 cross section from the difference spectrum (histogram) is 18 ± 4 μb/sr. Comparison with the singles analysis [Fig. 9(c) and Table II including 8.9, 9.4, and 10.6 MeV peaks] gives an overall γ_0 branch from the GQR of $4\pm1\times10^{-4}$. From the calculation and the integrated experimental cross section we obtain a total electromagnetic strength of $B(E2\uparrow)=6700\pm1400$ $e^2\text{fm}^4$ for the 10.6 MeV GQR, plus the 8.9 and 9.4 MeV 2^+ peaks. If we apply the standard picture, in which the resonance is taken to be a predominately isoscalar vibration with equal neutron and proton amplitudes, this $B(E2\uparrow)$ corresponds to $90\pm20\%$ of the isoscalar quadrupole EWSR. If we use the ratio of strengths from Table I we can extract $B(E2)\uparrow\approx5800$ for the 10.6 MeV peak. The angular correlation data of Fig. 7 is consistent with the relative $E1$ and $E2$ contributions obtained in this analysis (heavy solid line in Fig. 7).

VI. DECAYS TO EXCITED STATES

The experimental techniques employed in studying the branches from the giant resonance region to known bound states of ^{208}Pb were discussed in Sec. II. An instructive if somewhat qualitative picture of the branching to a few selected states is shown in Fig. 6. The top panel 6(a) shows the ground-state branch, while 6(b), 6(c), and 6(d) refer to branches to the 3^- 2.613, 2^+ 4.085, and 3^- 4.97 MeV states, respectively. Of particular note is the complete absence of any structure in the branches to the two low-lying collective states (2.61 and 4.085 MeV) in the giant resonance region. This seems especially surprising for the branch to the 2.6 MeV 3^- state, since the 10.6 MeV GQR makes up a significant fraction of the singles yield and could decay to the 2.6 MeV state via an $E1$ transition. A purely statistical estimate of this transition strength, made by assuming the $E1$ strength built on the 2.6 MeV state is distributed in the same way as that built on the ground state, would yield an $E1$ transition from the GQR approximately equal to its ground-state branch. In contrast the 3^- state at 4.97 MeV, which is thought to have a very noncollective character with a wavefunction dominated by a single particle hole configuration,[31] is strongly fed from the GQR region.

TABLE III. Relative photon branching to low-lying states in ^{208}Pb from an excitation energy region 9.5–11.5 MeV.

Final state		Decay branch relative to g.s.		
				Calculations
E_x	(MeV)	Experiment	Ref. 9	Ref. 10
0.0	0^+	1.0	1.0	1.0
2.61	3^-	0.04 ± 0.04	0.027	0.035
4.085	2^+	$0.02^{+0.05}_{-0.02}$		9×10^{-3}
4.97	3^-	1.80 ± 0.50		2.3[a]
5–7	1^-	1.15 ± 0.50		0.34

[a]Sum for three states at 4.7, 5.5, and 6.3 MeV.

In order to make a more quantitative investigation of the decay of the GQR region, cluster summed pulse height distributions were constructed for bins of excitation energy between 8.5 and 15.5 MeV. Peaks observed in these spectra were identified using the known decay scheme of ^{208}Pb.[12] The interpretation of the spectra was aided, where yield permitted, by further subdividing them according to the cluster multiplicity. The results for a bin spanning the peak of the GQR (9.5–11.5 MeV) are shown in Table III and Fig. 12. As in the qualitative branching spectra, the most striking feature is the absence of significant feeding to the 2.6 MeV 3^- state (i.e., a

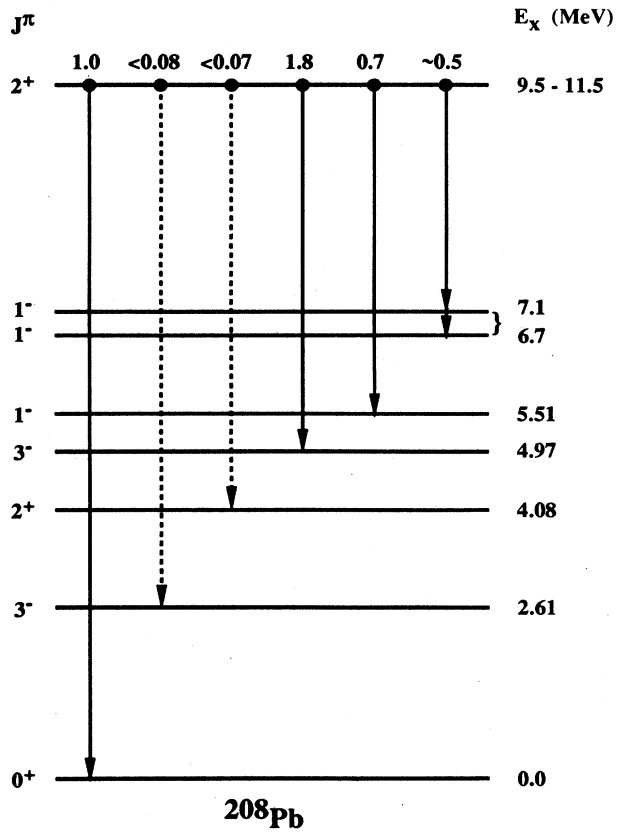

FIG. 12. Photon decay of the 9.5–11.5 MeV excitation energy region. Intensities relative to the ground-state branch are given across the top of the figure. Level energies are in MeV.

branch consistent with zero). The observed upper limit represents a suppression of more than an order of magnitude relative to strictly statistical predictions. The only decays from the GQR region strong enough to be clearly identified are branches to the 4.97 MeV 3^- and 5.512 MeV 1^- states. The latter is grouped in Table III with decays to other states tentatively identified with known 1^- levels near 7 MeV. The 5.5 MeV state accounts for about 60% of this yield. Decay to the 5^- state at 3.2 MeV was seen in the 8.5–9.5 MeV region and weaker evidence for decay to the 5^- state at 3.9 MeV in the 9.5–10.5 MeV region was found, confirming the presence of 4^+ or 6^+ strength in these excitation energy regions of ^{208}Pb. In the 12.5–15.5 MeV region, the only lines identified correspond to 1^- states[12] at 5.51, 7.06, and/or 7.08 MeV. This would be consistent with the photon decay mode expected from the giant monopole resonance which dominates the excitation cross section in this region.

VII. DISCUSSION OF RESULTS AND CONCLUSIONS

We have shown that the spectrum for inelastic scattering of ^{17}O on ^{208}Pb at 376 MeV can be described remarkably well using peak positions and strengths determined with 334 MeV proton scattering.[13] Since the relative cross sections resulting from these strengths are different in the two reactions, this should be regarded as strong corroboration of the (p,p') results.

The excitation of the IVGDR by hadronic probes has been a subject of considerable interest recently. It has even been suggested that standard methods employed in calculating this cross section greatly under estimate it.[32] This contention has been refuted in Ref. 15. Our data address this dispute. The predicted excitation of the IVGDR, calculated using the methods of Ref. 15, is shown in Fig. 9, and is clearly seen to be negligible. However if the inelastic spectrum is observed in coincidence with ground-state photon radiation, the contribution of the IVGDR can be clearly picked out. The corresponding experimental spectrum is shown in Fig. 11. Angular correlation data (Fig. 7) confirms an essentially pure $E1$ character above $\sim$12 MeV of excitation. By applying the multistep theory of nuclear reactions we were able to relate the ground-state photon production cross section to the IVGDR excitation cross section. It was found to agree with the predicted cross section within $\sim$15%, certainly within the combined uncertainty of the experiment and the calculation. It is interesting to point out that almost exact agreement with the measured cross section would be obtained if only Coulomb excitation were considered. As pointed out in Sec. III, the transition potential used for the nuclear part of the GDR excitation ignores the effect of the excess neutron in ^{17}O. Proper consideration of this effect is beyond the scope of this paper, but preliminary investigation indicates that it would result in a substantial ($\sim$50%) reduction in the nuclear contribution to the IVGDR cross section and a cross section at 14° within $\sim$5% of that obtained considering Coulomb excitation only.

By adjusting the calculated IVGDR contribution to the ground-state photon coincidence spectrum above 12 MeV of excitation, and then subtracting it from the data, we obtain a spectrum of excess ground-state photons peaked near 10 MeV, which is interpreted to result from the decay of the GQR. This interpretation is supported by gamma ray angular correlation data of Fig. 7. An analysis of ground-state photon decay in terms of the multistep reaction theory leads to an electromagnetic transition strength $B(E2)\uparrow = 6700 \pm 1400\ e^2\text{fm}^2$ for the 8.9, 9.3, and 10.6 MeV 2^+ states combined. This is more than 5 times larger than the value inferred from pion scattering in Ref. 33. Following the methods outlined in Sec. III we can use this result for $B(E2)\uparrow$, together with the depletion of the $L=2$ EWSR obtained in the singles analysis to obtain $M_n/M_p = 1.6 \pm 0.4$ which, in contrast to the results of Ref. 33, supports a predominantly isoscalar ($M_n/M_p = N/Z = 1.54$) character for this resonance. The 10.6 MeV state cannot be separated from the 9.3 and 8.9 MeV peaks in the experimental γ_0 data. If it contributes to the ground-state decay in the same proportion as its excitation strength we estimate $B(E2)\uparrow = 5800 \pm 1600\ e^2\text{fm}^4$ for the 10.6 peak alone (using excitation strength ratios from Table II).

The calculations using the multistep theory of nuclear reactions describe our data very well, in spite of the approximate nature of our application of the theory. Perhaps the comparative simplicity of gamma decay of a giant resonance state will prove to be a useful testing ground for more rigorous applications of this theory.

A final important, and at first sight surprising, result obtained from our data is the strong suppression of $E1$ transitions from the 10.6 MeV GQR to the 2.6 MeV 3^- state. In fact, just such a suppression has been predicted.[9,10] The calculation of Ref. 10 also makes predictions concerning a number of other branches from the GQR which agree reasonably well with our observation, as shown in Table III. An important contributing factor in both predictions of suppression of the GQR to 3^- transition is the cancellation between neutron and proton contributions to the decay resulting from the isoscalar character of both states. Any significant isovector admixture in the 10.6 MeV GQR should greatly enhance this decay branch. This datum therefore again supports a predominantly isoscalar 10.6 MeV GQR state.

It is interesting to note that the calculations shown in Fig. 10 suggest that the gamma decay of the GQR is dominated by decay from fully damped compound states. The predictions[9,10] of suppression of the GQR to 3^- transition are, however, based on wavefunctions of the undamped GQR state. We therefore conclude that the isospin character of the doorway state is preserved by the damping process.

This research was sponsored by the U.S. Department of Energy, under Contract No. DE-AC05-84OR21400 with Martin Marietta Energy Systems, Inc.

[1]G. R. Satchler, Phys. Rep. **14**, 99 (1974); F. E. Bertrand, Ann. Rev. Nucl. Sci. **26**, 457 (1976).
[2]K. Goeke and J. Speth, Ann. Rev. Nucl. Sci. **32**, 65 (1982).
[3]G. F. Bertsch, P. F. Bortignon, and R. A. Broglia, Rev. Mod. Phys. **55**, 287 (1983).
[4]P. F. Bortignon and R. A. Broglia, Nucl. Phys. **A371**, 405 (1981).
[5]G. J. Wagner, in *Giant Multipole Resonances,* edited by F. E. Bertrand (Harwood Academic, New York, 1980), pp. 251–274.
[6]L. S. Cardman, Nucl. Phys. **354**, 173c (1981).
[7]S. Brandenburg, W. T. A. Borghols, A. G. Drentje, L. P. Ekström, M. N. Harakeh, A. Van der Woude, A. Håkanson, L. Nilsson, N. Olsson, M. Pignanelli, and R. de Leo, Nucl. Phys. **A466**, 29 (1987).
[8]A. Bracco, Nucl. Phys. **A482**, 421c (1988).
[9]P. F. Bortignon, R. A. Broglia, and G. F. Bertsch, Phys. Lett. **148B**, 20 (1984).
[10]J. Speth, D. Cha, V. Klemt, and J. Wambach, Phys. Rev. C **31**, 2310 (1985).
[11]M. Jääskeläinen, D. G. Sarantites, R. Woodward, F. A. Dilmanian, J. T. Hood, R. Jääskeläinen, D. C. Hensley, M. L. Halbert, and J. H. Barker, Nucl. Instrum. Methods **204**, 385 (1983).
[12]M. J. Martin, Nucl. Data Sheets **47**, 797 (1986).
[13]G. R. Satchler, *Direct Nuclear Reactions* (Oxford University Press, Oxford, England, 1983); and Nucl. Phys. **A472**, 215 (1987).
[14]M. H. Macfarlane and S. C. Peiper, Argonne National Laboratory Report No. ANL-76-11, Rev. 1, 1978 (unpublished); M. Rhoades-Brown, M. H. Macfarlane, and S. C. Peiper, Phys. Rev. C **21**, 2417 (1980); **21**, 2436 (1980).
[15]A. Bohr and B. R. Mottleson, *Nuclear Structure* (Benjamin, Reading, MA, 1975), Vol. II.
[16]F. E. Bertrand, E. E. Gross, D. J. Horen, R. O. Sayer, T. P. Sjoreen, D. K. McDaniels, J. Lisantti, J. R. Tinsley, L. W. Swenson, J. B. McClelland, T. A. Carey, K. Jones, and S. J. Seestrom-Morris, Phys. Rev. C **34**, 45 (1986).
[17]T. P. Sjoreen, F. E. Bertrand, R. L. Auble, E. E. Gross, D. J. Horen, D. Shapira, and D. B. Wright, Phys. Rev. C **29**, 1370 (1984).
[18]A. Veyssiere, H. Beil, R. Bergere, P. Carlos, and A. Lepretre, Nucl. Phys. **A159**, 561 (1979).
[19]H. Feshbach, A. Kerman, and S. Koonin, Ann. Phys. **125**, 429 (1980); M. Hussein and K. McVoy, Phys. Rev. Lett. **43**, 1645 (1979); H. Dias, M. S. Hussein, and S. K. Adhikari, *ibid.* **57**, 1998 (1986).
[20]J. R. Beene, G. F. Bertsch, P. F. Bortignon, and R. A. Broglia, Phys. Lett. **B164**, 19 (1985).
[21]H. Dias, M. S. Hussein, B. V. Carlson, and A. C. Merchant, Phys. Lett. B **173**, 355 (1986).
[22]P. A. Moldauer, Phys. Rev. C **11**, 426 (1975).
[23]J. E. Lynn, *Theory of Neutron Resonance Cross Sections* (Oxford University Press, Oxford, England, 1968).
[24]P. Axel, K. K. Min, and D. C. Sutton, Phys. Rev. C **2**, 689 (1970).
[25]S. Raman, in *Neutron Capture Gamma-Ray Spectroscopy 1979,* edited by R. Chrien and W. Kane (Plenum, New York, 1979), p. 193; Phys. Rev. Lett. **40**, 1306 (1978).
[26]A. Gilbert and A. G. W. Cameron, Can. J. Phys. **43**, 1446 (1965).
[27]W. Dilg, W. Schantl, H. Vonach, and M. Uhl, Nucl. Phys. **A217**, 269 (1973).
[28]J. Rapaport, V. Kulkarni, and R. W. Finlay, Nucl. Phys. **A330**, 15 (1979).
[29]F. G. Perey and C. M. Perey, Atomic and Nucl. Data **13**, 293 (1974).
[30]S. G. Mughabghab M. Divadeenam, and N. E. Holden, *Neutron Cross Sections* (Academic, New York, 1981).
[31]M. B. Lewis, Nucl. Data Sheets **B5**, 243 (1971).
[32]R. J. Peterson, Phys. Rev. Lett. **57**, 1550 (1986).
[33]S. J. Seestrom-Morris, C. L. Morris, J. M. Moss, T. A. Carey, D. Drake, J.-C. Dousse, L. C. Bland, and G. S. Adams, Phys. Rev. C **33**, 1847 (1986).